

LYNX: Efficient MoE Inference Through Dynamic, Workload-agnostic Expert Reduction

Vima Gupta, Jae Hyung Ju, Kartik Sinha, Ada Gavrilovska, Anand Padmanabha Iyer

Georgia Institute of Technology
{vgupta345, jju35, ksinha45, ada, apadmanabh3}@gatech.edu

Abstract

Selective parameter activation provided by Mixture-of-Expert (MoE) models have made them a popular choice in modern foundational models. However, MoEs face a fundamental tension when employed for serving. *Batching*, critical for performance in serving, forces the activation of all experts, thereby negating MoEs’ benefits and exacerbating memory bandwidth bottlenecks. Existing work on efficient MoE inference are unable to resolve this tension even with extensive workload-specific tuning. We present LYNX, a system that enables efficient MoE inference in a *workload agnostic* fashion. Exploiting several key observations that we uncover in this work, LYNX provides a light-weight run-time dynamic expert remapping technique that depends only on information already available in the models. Our evaluation of LYNX on four state-of-the-art model families across nine benchmarks shows that it achieves up to $1.23\times$ improvement in throughput while simultaneously improving accuracy by up to 4% in the majority of the tasks, and incurs only a negligible accuracy loss of less than 1% points in significantly hard tasks. Further, LYNX is complementary to existing techniques where it additionally boosts their performance by up to $1.38\times$.

1 Introduction

Mixture-of-Experts (MoE) has become the defacto architecture in foundational models, powering the majority of the state-of-the-art offerings from families such as Qwen [55], Llama [39], Mixtral [25, 40] and Deepseek [11, 46]. MoEs decompose the dense feed forward layer with multiple subnetworks known as *experts*, and a gating network that routes each input token to a small subset of these experts [20, 22, 28, 48]. Such *selective* activations of experts enable MoEs to be more FLOP efficient per parameter [32, 48] and thus allow scaling the total model parameters with only a sublinear increase in computational cost.

The selective parameter activation characteristic of MoEs is not just beneficial for training, but it is also useful during inference. Since an input only activates a small fraction of the total parameters—for instance, each input in Mixtral only activates 12.9 billion out of its total 47 billion parameters [25]—MoEs potentially reduce the *per-input* computational requirements of inference. While such reduction in computation can bring in desirable latency reduction in many serving scenarios, MoEs face a fundamental challenge when employed for large-scale inference.

Production grade services such as OpenAI’s ChatGPT [1, 43] and Anthropic’s Claude [4] are required to handle millions of concurrent requests. To support high load, these services employ *request batching* [30, 57], where multiple requests are combined and executed together to improve efficiency. Unfortunately, batching is at odds with the very premise of MoEs; since each input in a batch *independently* invokes experts, even a small batch can end up activating all the experts. As an example, an MoE model with 64 experts where each input activates eight experts, a batch of eight is sufficient to activate all 64 experts [55]. This is problematic due to two reasons. First, an MoE model typically contains more parameters compared to a dense model¹, thus requiring more GPU memory leading to *memory pressure*. Second, to execute a *layer*, MoE models incur the cost of moving the experts needed by the batch from the GPU’s High Bandwidth Memory (HBM) to its Streaming Multiprocessors (SM). Thus, MoE inference is fundamentally constrained by the *memory bandwidth*, where the latency is dictated by the total experts activated by a batch.

Existing work on MoE inference efficiency (§6) has mainly focused on alleviating the memory pressure, and can be classified into two broad categories. *Lossless* techniques [23, 53, 58] preserve the accuracy of the model by *offloading* experts outside the GPU to reduce memory requirements, and propose ways to fetch them just-in-time or intelligently based on prediction. Selective expert fetching in offloading techniques incur the cost of parameter movement between the memory hierarchy (e.g., GPU-CPU), making them unsuitable for batched inference scenarios. *Lossy* techniques can trade-off accuracy for memory savings by *reducing* the total number and/or size of the experts in the model use approaches such as pruning [12, 31, 38], quantization [8, 21] and clustering [17, 34, 56]. Such approaches rely heavily on calibration datasets and extensive tuning and suffer from accuracy degradation in complex reasoning tasks such as GSM8k or HumanEval (§2). More recent works have argued for dynamically reducing the number of experts at a per-sequence-basis [8, 21, 38]. Since they make decisions at a per-input basis and not at the batch level, their benefits are sensitive to the model sparsity ratio and quickly shrink as batch sizes grow.

In this paper, we present LYNX, the first system to the best of our knowledge that enables efficient MoE inference by alleviating the memory bandwidth bottleneck in a *workload-*

¹An MoE with E experts each with P parameters generally underperform a dense model with $E \times P$ parameters [9, 29].

agnostic fashion: without the need for calibration datasets or knowledge of the workload. The key idea in LYNX is to reduce the total number of experts invoked at a *batch-level* through *run-time dynamic expert remapping*. LYNX focuses on deployments where the request rate warrants batching and large batches are the norm [59]. We have designed LYNX to be a plug-and-play framework that does not change the semantics of the model’s execution or its architecture. Further, LYNX’s techniques introduce no dependency and work based on information already available in the models. Consequently, the techniques we present in this paper are generalizable to any model and workload combination, and is complementary to existing work on MoE optimization, including pruning, offload and quantization. (§5).

To achieve its goal, LYNX must address several challenges. First, LYNX needs to determine which inputs in the batch are amenable to expert remapping. Since our guiding principle is to be workload and model agnostic, it is not feasible to depend on such task or model specific calibration. Second, any modifications to the token to expert mapping affects the accuracy of the output. Therefore, LYNX must understand the effect of accuracy on remapping, again, without depending on task or model specific techniques. Third, naively remapping the experts per input may not lead to a reduction in experts at the batch-level, hence LYNX must consider the batch as a whole (§2.3). Finally, LYNX’s focus on practical large-scale deployments means that all of these must happen at run-time. Therefore, LYNX must work in the critical path of inference and hence incur minimal overheads.

Towards building a solution by resolving these challenges, LYNX uncovers and exploits a number of observations. To remain workload-agnostic, LYNX depends only on information that is already available in state-of-the-art MoE models. In particular, we identify that the confidence scores computed by an MoE model’s router for an input is highly indicative of its amenability to remapping (§3.1). Further, we observe that the sorted order of the experts from which the top-k is chosen by the routers in MoE models provide hints on the accuracy (§3.2). Specifically, across several model families, we uncover that the first expert disproportionately contributes towards output quality compared to other as shown in Figure 6. In addition, our exhaustive analysis reveal that expert selection is highly sensitive to the inference phase, with prefill showing high sensitivity while decode demonstrates remarkable resilience. (§3.3)

Equipped with this knowledge, LYNX’s confidence analyzer (§3.1) develops a simple technique that is robust in identifying inputs in a batch whose experts can be remapped. Once these inputs are identified, LYNX’s adaptive expert scorer (§3.2) then determines which experts can be remapped for each input. It does this as a joint optimization where it determines the input-expert remap for all the inputs in the batch and then determines the combination that minimizes the total experts invoked by the batch while minimizing the accuracy

loss. By default, LYNX emphasizes accuracy preservation, but due to the nature of how it works, LYNX can enable the user to traverse the accuracy-performance curve (§5.3). Since performance is paramount to LYNX as a critical path solution, we implement it in CUDA kernels that intercept the router output at every layer with minimal overheads (§4).

We have implemented LYNX on vLLM [30] and evaluated it on the state-of-the-art models from four families—Qwen [55], Deepseek [46], Mixtral [25] and Llama [39]—on nine benchmarks ranging from easy to hard. Across these models and benchmarks, LYNX improves throughput by up to $1.23\times$ while incurring minimal to no accuracy loss. Notably, LYNX improves the accuracy by up to four percentage points on many tasks. In difficult benchmarks such as GSM8k, where the model families themselves exhibit a 8% point standard deviation, LYNX incurs less than 1 percent point accuracy loss. The benefits of LYNX is consistent across model families and benchmarks, and even extends to cutting edge releases from these families which have made MoE based optimizations a top priority. Further, the workload agnostic nature of LYNX shows remarkable compatibility with existing MoE optimization techniques, where it boosts the performance of the state-of-the-art offloading and compression techniques by 38% and 15%, respectively. Finally, LYNX’s techniques become more important as the disparity between compute and memory bandwidth continues to increase between current and future GPUs.

2 Background & Challenges

Large language models process input using two distinct phases: prefill and decode. During prefill, the model processes the input prompt in parallel, generating hidden states (or the KV cache) that capture the input context. The decode phase then generates output tokens one at a time, using these hidden states along with previously generated tokens. This autoregressive generation means that decode iterations typically dominate serving costs in production deployments for generative tasks. As models grow larger, serving them efficiently becomes increasingly challenging.

2.1 MoE Architecture and Serving

The key principle behind MoEs is selective computation. MoEs use specialized sub-networks (experts) that are selectively activated based on input characteristics. A router network examines each input token and directs it to the most relevant experts. The expert selection process follows a two-step approach. First, the router network computes logits for each expert, which are transformed into selection probabilities through softmax normalization:

$$p_i = \frac{e^{z_i}}{\sum_{j=1}^N e^{z_j}} \quad (1)$$

where p_i represents the probability of selecting expert i , z_i is the router logit for expert i , and N is the to-

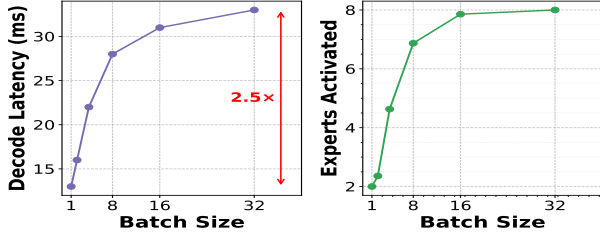


Figure 1: Impact of batching on decode latency. Even at modest batch sizes (8-16), all experts are activated, forcing memory fetch of all model parameters. **Left:** Decode latency increases 2.5 \times as batch size grows from 1 to 32, as larger number of experts are activated. **Right:** Number of activated experts rapidly saturates to maximum (8) with increasing batch size.

tal number of experts. The model then selects the k experts with highest routing probabilities: $E(x) = \{i \in 1, \dots, N : p_i \text{ is among top } k \text{ values}\}$, where $E(x)$ represents the set of selected experts for input token x . To understand whether our workload is compute-intensive or memory-intensive, we study the arithmetic intensity of MoE models as a function of the model parameters. It is a direct indicator of how well memory access costs can be hidden behind computation. The arithmetic intensity (operations per byte) during MoE inference exposes this fundamental challenge of memory boundedness of decode phase. Here k is the number of experts activated per token, $total_num_experts$ shows the total number of experts per layer and n indicates the total number of tokens in the given batch.

$$\text{Arithmetic Intensity} \approx \frac{n \cdot k}{total_num_experts} \quad (2)$$

Modern LLM serving systems must process multiple requests simultaneously [30, 57]. Because the load-balancing loss encourages different tokens in a batch to activate different experts, even moderate batch sizes (e.g., 16). In Figure 1, we measure the impact of batching on decode latency and show how it correlates with number of activated experts per batch for Mixtral-8x7B-v0.1 (bf-16).

Unlike dense models where operations amortize weight fetching across many tokens, MoE models suffer from reduced arithmetic intensity that scales inversely with expert count. During prefill, the number of tokens is large enough to stay compute-bound while during batched decode, the number of tokens is much smaller.

In Figure 2, we measure how iteration latency in MoEs varies with the number of activated experts during the prefill vs. the decode phase. Here we artificially control the number of activated parameters to generate the latency trends. Figure 2 shows that in batched serving scenarios, latency cost of MoEs is proportional to the model size and not the subset of experts activated for each token during decode phase while remains similar during prefill phase. This can be attributed to the memory-bound nature of decode phase where majority of the time is spent in fetching expert parameters from the memory.

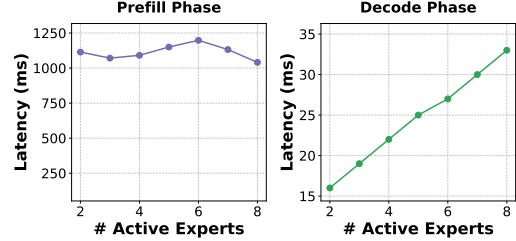


Figure 2: Left: Prefill latency remains relatively constant (~ 1100 ms) regardless of active experts, shows compute-bound behavior. **Right:** Decode latency scales linearly with the number of active experts, revealing memory bandwidth as the bottleneck.

Takeaway 1: During the memory-bound decode phase, the latency in MoE’s scales with total number of expert parameters rather than activated parameters, rendering them inefficient at inference.

2.2 Expert Activation Patterns

Expert assignment for each token is determined at runtime by the router’s softmax probabilities. During training, auxiliary load balancing losses encourage uniform expert utilization [48]. Our analysis of expert activation across millions of tokens from the ShareGPT-V3 dataset confirms this uniformity - when examined at scale, no expert stands out as consistently underutilized [25, 38].

However, examining activation patterns at batch-level granularity tells a different story. For iteration-level scheduling, which is the norm in LLM inference systems [30], the composition of input batches varies from one iteration to the next. This dynamic batch composition leads to significant variation in which experts are activated, even though the aggregate distribution remains uniform. The variability in expert activation is significantly higher at individual batch level as compared to the aggregate. Identifying permanently underutilized experts is quite challenging and requires prior knowledge of the workload. The strong batch-level skew in expert activation hints at the possibility of dynamic expert management during serving time to reduce decode latency.

Takeaway 2: Expert activation shows strong heterogeneity at batch-level despite being uniform at an aggregate level.

2.3 Challenges

As shown in Takeaway-1, MoE inference latency scales with the number of activated parameters for the batch, rather than individual tokens. To reduce this associated data movement cost, we need to reduce the set of activated experts per batch. MoE training incentivizes all experts to acquire some relevant knowledge. This is accomplished through an auxiliary load-balancing loss function [11]. As observed in Figure 3, during the course of running a benchmark, almost all experts are activated uniformly. Existing pruning techniques rely on using the

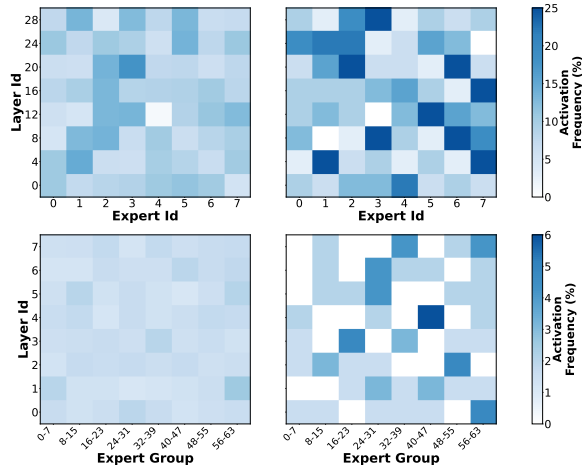


Figure 3: Comparison of expert activation patterns across different granularities: (Left) aggregate dataset-level uniformity, (Right) batch-level skew for Mixtral 8X7B (Upper) and Qwen2 (Lower) (combined experts for readability)

expert activation signature of a calibration dataset to remove some experts [12]. While this is an enticing approach, such techniques run the risk of significant accuracy drops when run on workloads with a different expert activation signature as compared to the calibration dataset.

Identifying Important Tokens. At each iteration of the batch, giving the same importance to expert choice of each token would end up activating almost all experts. Thus, we need a notion of *relative importance* of expert choice between different tokens in the batch. Experts in an MoE are more or less relevant depending on the task [24] and sequence at hand. Thus, we need to identify tokens who require their selected experts for an accurate output, to ensure we do not drop their experts. Conversely, we need the set of tokens within the batch for which replacing some of their top-k experts would not result in quality degradation. This leads to our first challenge: *How can we identify tokens that are amenable to modifying expert mapping without accuracy loss?*

Selecting critical Experts for a Batch. Even if we know which tokens are amenable to dropping experts, we need to drop only those experts that are not critical for *any* token. That is, if an expert is non-critical for a certain token but is important for others, dropping it may degrade accuracy. One measure of relative expert importance for a token is the expert weight assigned due to top-k; less important experts would have less weight. However, we need to reconcile expert weights, which are per-token, with all of the experts that are activated due to all (important) tokens in the batch, leading to our second challenge: *How can we find the minimal set of experts needed for a given batch of tokens?*

Opportunistic Expert Reduction. A scheme may always drop non-critical experts, but doing so may not be always beneficial for performance. For example, for compute-bound scenarios, even aggressive expert dropping may end up activating all experts while risking accuracy degradation. Such

scenarios can arise, for example, during times of high system load or during prefill. We need to accurately analyze scenarios where inference is memory bound, and where dropping experts would yield meaningful speedup. Thus, our third challenge is: *How can we reliably detect opportunities for speedup while avoiding unnecessary performance drop during different phases of inference?*

Addressing these challenges requires a fundamental understanding of how expert selection impacts accuracy across multiple granularities: individual tokens, batches, layers, and complete inference iterations. To enable a plug and play solution, our policy must not depend on workload characteristics, as request types can drift over time in deployments. Finally, for a technique to achieve meaningful real-world speedup, our policy must work with state-of-the-art MoEs running on production systems. As expert selection is a layer-level problem, our solution must be lightweight so it runs efficiently on the GPU, and adaptive to various model families. Only through a multi-faceted analysis can we develop principled approaches to expert reduction that balance performance gains with accuracy preservation.

3 LYNX Design

LYNX is an MoE inference serving system that integrates with any existing LLM serving engine for low-latency applications. LYNX identifies that in memory-bound phases, inference latency depends on the total experts activated by the batch, rather than individual tokens. LYNX selectively identifies such memory-bound phases and applies expert reduction to those which maximize the performance benefit while maintaining iso-accuracy as vanilla model serving.

LYNX focuses on reducing this final set of activated experts at the batch-level granularity. Our key insight is in identifying unimportant token-to-expert mappings at each layer which can be modified without impacting downstream tasks while being workload-agnostic. LYNX identifies this heterogeneity in the importance of token-to-expert mapping at various hierarchies, at the per-token, per-batch and per-iteration level during model serving. LYNX then creates a minimal set of experts that need to be activated and remaps the remaining token-to-expert mappings. LYNX leverages these heterogeneous trends to dynamically activate a reduced final set of experts without any recalibration. We illustrate these trends and explain how they guide our design choices using Qwen2-57B-A14B, DeepSeek-V2-Lite-Chat and Mixtral-8x7B-v0.1 with GSM8K and HumanEval as the benchmarks.

3.1 Are tokens in a batch equally important?

The router network in MoEs serves a critical role in matching tokens with appropriate experts. While most works treat router decisions as binary selections, our investigation reveals that the router’s confidence in these selections carries crucial information about how different tokens interact with the expert pool. To quantify this relationship, we analyzed how router

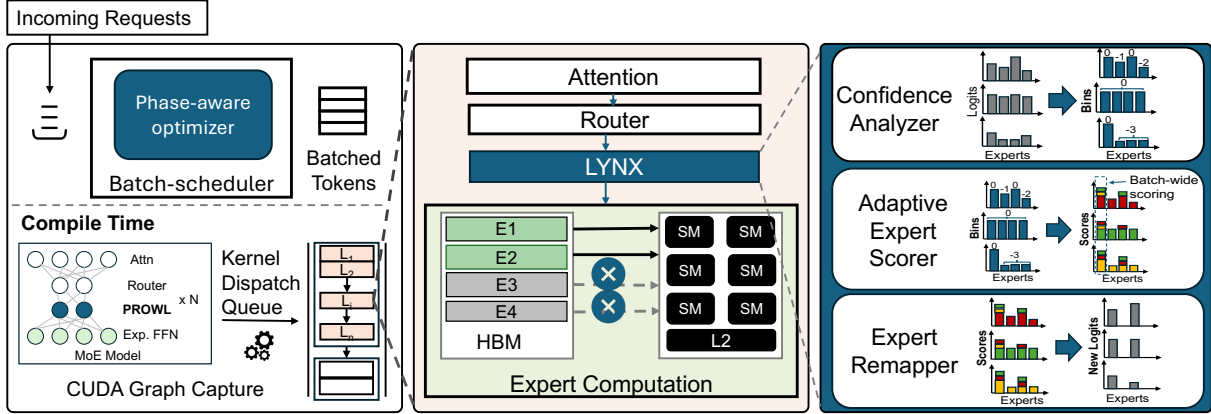


Figure 4: System architecture of LYNX design. Left: Phase-aware optimizer identifies memory-bound inference phases; layer-level components are compiled using CUDA Graphs for maximum performance. Center: LYNX results in much less experts being activated, reducing memory traffic (two out of four activated in this example). Right: LYNX first bins expert choices of each token, then develops batch-wide scores for each expert, selecting the critical experts, and finally remaps expert choice of all tokens to the critical expert set.

confidence correlates with a token’s sensitivity to expert reassignment. We developed a systematic way to measure router confidence and studied how tokens with different confidence levels respond to modifications in their expert assignments.

Figure 5 uncovers a fundamental pattern in this relationship. We quantify router confidence per token as the variance in the normalized probability scores. As we vary confidence thresholds, we observe a clear and growing separation between how high and low confidence tokens respond to expert reassignment. High confidence tokens consistently demonstrate greater sensitivity to changes in expert assignment, while low confidence tokens show lower accuracy degradation. The diverging trends as confidence increases suggest the router logits contain a meaningful signal for distinguishing critical token-expert mappings from more flexible ones.

Insight 1: Router confidence provides a reliable signal for identifying critical token-expert mappings, to ensure expert reassignment has minimal impact on downstream accuracy.

Based on this observation, not all tokens require the same level of computational precision. Thus, we extract ‘important’ tokens which are highly sensitive to expert reassignment and prioritize retaining their expert selection while allowing reassignment for the remainder of the tokens in the batch.

3.1.1 Confidence analyzer

As shown in Figure 4, the role of the confidence analyzer is to separate high confidence tokens from low confidence tokens (refer to Insight 3.1). The confidence analyzer intercepts the tokens at every MoE layer after they have been passed through the router network §2.2. The router network generates routing logits, which are raw numerical scores. These routing logits are processed to generate probability weights between 0 and 1 to indicate the likelihood of the given token being mapped

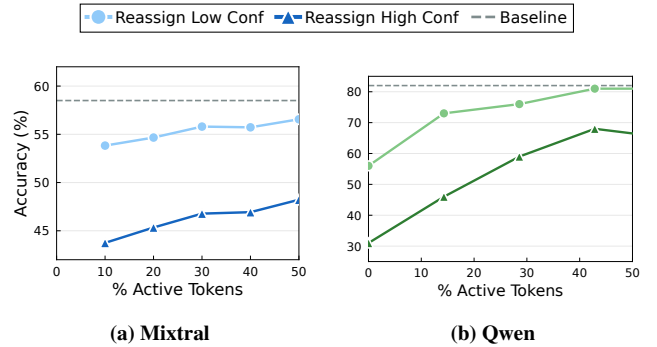


Figure 5: Impact of token confidence on accuracy for selective expert routing. Reassigning high confidence tokens maintains better accuracy than reassigning low confidence tokens.

to the given expert. The confidence analyzer intercepts these probability weights and measures the affinity of each expert to the top-1 expert for that token. Because the probabilities after softmax are proportional to the exponential of logits, we must subtract two logits to obtain the log of the corresponding probability ratio. To measure this affinity, the confidence analyzer performs binning of these values into discrete bins. The bin values start from 0, indicating highest affinity to the top-1 expert probability weight, and the bin value becomes negative as the difference between the expert weight and top-1 weight increases (Figure 4). In order to generalize the policy across models with different number of experts and different sparsity ratios, we introduce two configuration parameters, namely α and β (§A). For a given model, the width of each bin is inversely proportional to α , and β captures the maximum allowed number of bins. These configuration knobs are set for a given model architecture. They enable us to adapt any model given its sparsity ratio (top-k/n). After testing multiple measures of confidence like variance, entropy and gini-index, we chose the ratio of expert probability to the top-1 expert probability as the most intuitive and representative measure.

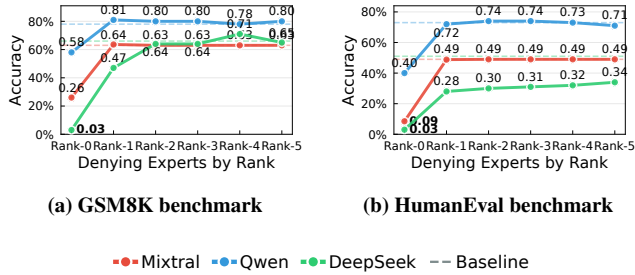


Figure 6: Impact of denying experts by rank on model accuracy. Expert 0 (E0) is critical for performance across all models.

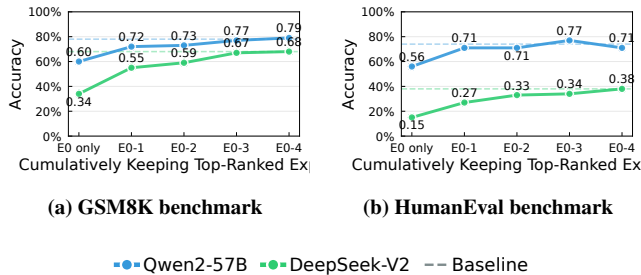


Figure 7: Accuracy when cumulatively keeping top-ranked experts. Diminishing returns are observed after keeping 3-4 experts, with most performance recovered.

3.2 Are all top- k experts and layers equal?

Figures 6 and 7 quantify this hierarchy by showing the impact of reassigning experts on downstream accuracy. The results reveal a striking asymmetry: modifying primary expert assignments devastates model performance while changes to secondary expert selection cause minimal disruption. Most telling is the consistency of this pattern across different evaluation criteria - it reflects a fundamental property of how MoEs process information rather than an artifact of measurement.

This finding challenges our basic assumptions about MoE operation. The model doesn't actually need equal contribution from all selected experts - it relies heavily on primary selections while maintaining substantial redundancy in secondary choices. This variation in expert importance suggests that treating all expert computations equally during serving leaves significant optimization potential untapped.

Insight 2: The top ranking expert dominates output quality, with lower-ranked experts among $top-k$ showing high redundancy.

In LYNX, we leverage this insight of not all $top-k$ experts being equally important, to reduce the final set of activated experts for a given batch of tokens. Instead of retaining all $top-k$ experts for tokens across the batch, we prioritize experts that were in lower bins and thereby had more affinity to the top-1 expert. Moreover, layer-wise sensitivity analysis (shown in Figure 8) shows that we can aggressively reduce more experts in certain layers compared to others.

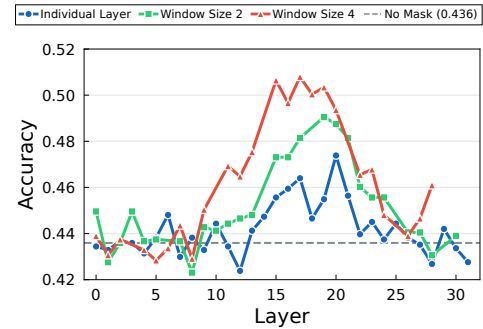


Figure 8: Layer-wise sensitivity analysis shows accuracy degradation when preserving expert assignments for a sliding window while masking others, suggesting the need for aggressive pruning in less sensitive layers while preserving experts in critical layers.

3.2.1 Adaptive expert scorer

This component receives the confidence scores, the token-to-expert probability scores, and the memory-bound flag populated by the phase-aware optimizer as input. Using these inputs, this component determines which experts should be retained in the set of final activated experts such that there is least impact on downstream accuracy. We implement a batch-wide scoring algorithm. For each expert, we add a weighted score to its router logit based on how frequently other tokens in the same batch preferred that expert. Unlike vanilla weighted averaging, we use the batch size as the base of our exponential and raise it to the bin-value assigned to expert based on the output of the confidence analyzer. Thereby, the expert scorer dynamically determines how many experts are finally activated based on the router logits, the width of each bin and the number of allowed bins. Based on our findings from Insight 3.2, the high confidence tokens are mapped to their first preference of expert to ensure minimal accuracy drop. For newer MoE architectures [11, 46] with shared experts that are activated at every layer and routed experts that are selected dynamically, LYNX ensures that the shared experts are always included in the final set of activated experts with the probability score of 1.

3.3 Are phases equally sensitive to experts?

Perhaps our most surprising discovery shows how MoE behavior varies across different inference phases. The prevailing view treats expert selection as equally important throughout inference. Our investigation reveals this assumption significantly mischaracterizes how MoEs actually process information. To understand this phenomenon, we conducted a systematic comparison of how expert reassignment impacts model behavior during prefill versus decode phases. The experiment measured accuracy across different types of tasks, specifically chosen to stress different aspects of model capability.

Figure 9 reveals a striking asymmetry that persists across diverse workloads. Expert reassignment during prefill phase substantially impacts model performance on both code generation (HumanEval) and complex reasoning problems (GSM8K). In

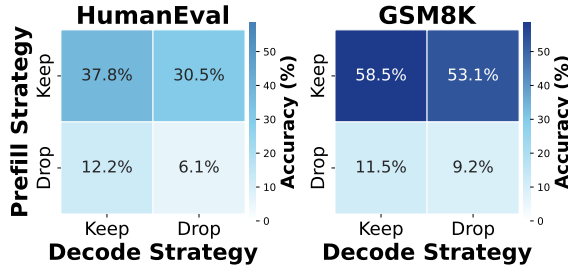


Figure 9: Phase-specific impact of expert reassignment across different tasks. Code generation (HumanEval) and reasoning-heavy tasks (GSM8K) both show sensitivity during prefill but resilience during decode, revealing a fundamental asymmetry in how MoEs process information across phases.

contrast, similar modifications during decode show minimal impact across all task types. This consistency across such different types of computation suggests we’ve uncovered a fundamental property of how MoEs process information rather than a task-specific phenomenon.

The explanation lies in the nature of autoregressive inference - the prefill phase establishes critical context that guides all subsequent computation, while the decode phase benefits from multiple mechanisms (attention, residual connections) that can compensate for suboptimal expert selection.

Insight 3: MoEs exhibit fundamentally different sensitivity to expert selection during prefill versus decode phases, enabling phase-specific optimization strategies.

3.3.1 Phase-aware optimizer

Most LLM serving engines like *Orca*, *vLLM* and *SGLang* use continuous batching to dynamically create input token batches from incoming requests. The batch scheduler creates and dispatches this input token batch for the forward pass on the model. The phase-aware optimizer works with the batch scheduler to identify whether a given batch of tokens is compute-bound or memory bound. In scheduling policies, where prefill and decode batches are not mixed but co-located, the phase-aware optimizer simply identifies the decode batch as memory-bound and populates a flag to indicate this memory-boundedness to the future components. In order to meet tight SLA constraints, LLMs are typically deployed through prefill-decode disaggregation where prefills and decode operations are scheduled on separate instances within the same replica. Here the phase-optimizer simply determines which is the decode instance and marks it as memory-bounded. For policies like chunked prefills, where the same batch can have both prefill and decode tokens, we specifically identify batches with only decode tokens and label those as memory-bound. There might be scenarios where the chunk size for the prefill is small enough to be memory-bound but that might adversely impact TTFT. We leave tackling those scenarios for future work. Using the insight that prefill is more sensitive to

preserving expert-mapping as compared to decode, the phase-aware optimizer selectively applies LYNX’s optimizations.

3.4 Expert Remapper

The expert remapper takes as input the final number of experts to activate from the Adaptive Expert Scorer and their probability scores. This component determines the new expert mapping for tokens whose previous expert mappings are deemed as less confident. Every low confidence token is remapped to the final set of selected experts determined by previous stage. The new probability scores are then used to determine the final token-to-expert assignments. This component triggers the launch of the expert computation kernel along with the optimal kernel dispatch parameters.

LYNX reduces the number of experts activated at runtime by reassigning the token to expert mappings. Unlike prior works that reduce the computation per token, LYNX remaps the expert selection to pick overlapping experts, retaining top-k based expert selection for each token. The goal of our technique is to effectively reduce the total set of activated experts while keeping the number of experts per token same as the baseline. Instead of making predictions based on a calibration dataset, LYNX uses a lightweight runtime mechanism that results in lower expert activations at the batch-level granularity. LYNX remains workload-agnostic and can adapt to different types of MoE architectures out-of-the-box.

These three properties - varying expert importance, token-level sensitivity, and phase-specific behavior - collectively inspire the design for various components in LYNX. The consistency of these patterns across different evaluation settings, tasks, and model scales suggests we’ve uncovered fundamental properties of MoE computation rather than implementation artifacts. This understanding reveals that efficient MoE serving requires adaptive decision-making that can respond to these variations at different deployment scales.

3.5 Architecture and Workflow

Figure 4 presents the system architecture overview of LYNX, showing how its components interact with the inference engine at different stages. The phase-aware optimizer operates within the batch scheduler of the inference engine. The remaining components, namely confidence analyzer, adaptive expert scorer and expert remapper are integrated within the control plane of the LLM DAG and operate at per-layer granularity. The confidence analyzer intercepts the routing decision from the router at every layer. The adaptive expert scorer determines how many experts will be activated for a given layer based on the initial routing decision and the output from the confidence analyzer. The expert remapper modifies the initially intercepted routing logits and launches the expert computation kernel for the layer.

LYNX comprises four components. For an incoming batch of tokens, the phase aware optimizer (Figure 4 left) selectively applies our techniques to memory-bound phases. The batch

scheduler creates a batch of tokens to be scheduled in the next iteration via continuous batching. The optimizer identifies if the scheduled batch is compute-bound or memory-bound based on the number of tokens in the batch. If the batch is compute-bound, such as during prefills which is characterized by long input lengths, there is no benefit from reducing experts and LYNX’s techniques are skipped for that iteration.

For a memory-bound iteration, LYNX remaps the expert preferences for the batch of tokens. We note that memory bound decode forms majority of batch iterations for long decoding tasks. The MoE router for a given layer generates the expert selection logits, which forms the input for the confidence analyzer. The confidence-analyzer bins the router logit values. The adaptive expert selector component unmaps experts with low activation frequency across the remaining high-priority tokens, and the expert remapper maps the final set of tokens to a reduced expert pool while preserving critical token-expert relationships. This dynamic workflow enables batch-level optimization of expert computation without requiring model modifications or offline tuning.

4 Implementation

LYNX seamlessly integrates with any LLM serving engine while minimizing overhead in the token generation critical path. Our implementation extends vLLM [30] with minimal modifications to the scheduler, where it is tightly coupled to enable phase-aware optimization and applied selectively to memory-bound phases during inference. LYNX’s components are implemented using four fused Triton [51] kernels.

Each kernel in LYNX fuses operations that would otherwise launch multiple PyTorch kernels, eliminating intermediate tensors and excess memory traffic by keeping computations in registers or shared memory. This design reduces memory accesses, cuts kernel launch overhead, and maintains static control flow for efficient CUDAGraph capture. The routing policy is implemented in four steps: token-wise binning, batch-wise scoring, expert pruning, and expert remapping. The first kernel discretizes logits and computes top-k weight sums, the next two score and prune experts before recomputing softmax and top-k, and the final kernel compacts the active-expert list, assigns tokens, and renormalizes weights. Together, these four kernels replace dozens of small PyTorch operations with a few efficient launches (Figure 15).

Finally, the effectiveness of LYNX depends on whether inference is memory bound. Scheduling policies like prefill-first [57] and decode-first [42] optimize different metrics, such as time to first token (TTFT) and time between tokens (TBT). In disaggregated serving, compute-bound prefill and memory-bound decode phases run on separate instances [61] to improve utilization, while throughput-oriented methods like SarathiServe [3] overlap prefill and decode phases to raise arithmetic intensity. Although LYNX targets latency-sensitive applications, it also benefits throughput oriented policies like chunked-prefill by reducing decode latency in

decode-only batches. Using the phase-aware optimizer, LYNX identifies such opportunities and can integrate with any inference engine since it only optimizes memory-bound phases. We demonstrate this behavior on vLLM, where chunked prefill is enabled by default.

LYNX prioritizes deployment simplicity. Users can enable all optimizations through a single CLI flag without modifying the model or runtime. The system automatically selects kernel configurations based on the number of active experts and available hardware, delivering immediate performance gains across diverse serving environments.

5 Evaluation

We evaluate LYNX on state-of-the-art models from four families across nine benchmarks (§5.1). Our key findings are:

- LYNX provides up to $1.23\times$ improvements in performance with minimal to no loss in accuracy in the vast majority of the benchmarks. Strikingly, LYNX improves the accuracy in many tasks. In hard tasks such as GSM8k, where model families exhibit variations of up to 8%, LYNX is able to achieve performance benefits by only incurring less than 1% point accuracy loss.
- When applied atop, LYNX boosts the performance of Fiddler [26], a SOTA offloading technique, and LLM compressor’s SmoothQuant [52], a SOTA compression technique, by 38 and 12 % points, respectively, highlighting its complementary nature to existing approaches. (§5.5)
- LYNX is able to retain its performance on different batch sizes due to its batch-aware expert remapping. Further, LYNX’s overheads are consistently less than 3% across sequence lengths and batch sizes, even with it being on the critical path. (§5.6, §5.7)

5.1 Experimental Setup

Models and Experimental Setup. We evaluate LYNX across models from four families: Qwen [55], Llama [39], DeepSeek [11] and Mixtral [25]. Specifically, we use Qwen2-57B-A14B-Instruct, Qwen3-235B-A22B-Instruct-2507, Mixtral-8x7B-Instruct-v0.1, DeepSeek-V2-Lite-Chat and Llama-4-Maverick-17B-128E-Instruct [25, 47, 55]. We use 8x NVIDIA H200 GPUs (143771 MiB memory each) connected using SXM NVLink to conduct all our experiments unless otherwise stated. The machine is equipped with 2x AMD EPYC 9554 64-Core Processors (128 cores total) and 1.5 TB DRAM, running Ubuntu 22.04.4 LTS, with NVIDIA driver 560.35.05 and CUDA 12.6. Based on our conversations with our industry collaborators, this configuration reflects those used in real-world production deployments. Mixtral-8x7B-Instruct-v0.1 and Qwen2-57B-A14B were run with a tensor parallelism degree of two. Experiments for Deepseek-V2-Lite-Chat were conducted on a single GPU due to its feasibly smaller model parameter count. Llama-4-Maverick-17B-128E-Instruct and

Qwen3-235B-A22B-Instruct-2507 were run with tensor parallel degree of four. All experiments were run in an online serving setting with the latest stable vllm version (v0.10.1) through EleutherAI’s LM evaluation harness. The model and inference engine configuration is in line with and represents the way these models are deployed in practice [2, 14, 50].

Workload. We measure the efficacy of LYNX’s policies on nine generative tasks with varying prefill to decode lengths with an emphasis on long generation tasks. GSM8K [10] is a diverse grade school math word problems task which measures a model’s ability to solve multi-step mathematical reasoning problems. HumanEval [6] is a benchmark designed to evaluate an LLM’s code generation capabilities through hand-crafted programming challenges. MBPP [5] is a comprehensive Python code generation benchmark consisting of hand-written problems with associated test cases. Minerva Math Algebra [33] is a benchmark designed to evaluate mathematical reasoning and problem-solving abilities in algebraic domains. TruthfulQA [36] is a zero-shot generative benchmark which measures the truthfulness of models when generating answers to adversarial questions that expose common human misconceptions. CoQA (Conversational Question Answering) [45] is a large-scale dataset which evaluates a model’s ability to participate in multi-turn QA dialogues. NarrativeQA [27] is a reading-comprehension benchmark which tests a model’s long-form narrative understanding by asking free-form questions about full book or movie script summaries. The Stanford Question Answering Dataset (SQuAD) [44] evaluates span-based machine reading comprehension on 100k+ Wikipedia articles. CNN/DailyMail (CNN/DM) [19] is a news summarization benchmark pairing single-document inputs with multi-sentence abstractive and highlight summaries.

Metrics. We report the speedup in throughput numbers for LYNX versus vanilla model serving, measured as tokens/sec. The time per output token metric can be inferred as the inverse of the throughput value. We also report raw throughput numbers across models and benchmarks. For accuracy, we pick the most appropriate metric as reported for ML tasks and for details like number of fewshot examples and other benchmarking practices, we follow the guidelines from EleutherAI’s benchmarking harness. We measure token throughput using the metrics generated by the standard vllm benchmarking harness. In addition to system level data, we also capture the kernel-level latencies using Perfetto for graph capture iteration latencies.

5.2 Accuracy & Throughput Benefits

Figure 10 compares LYNX with vanilla model serving across reasoning and NLP workloads. Overall, LYNX significantly improves throughput while adhering to tight accuracy budget, and in several cases even improves accuracy.

Median speedups range from 10.0–23.4% for reasoning workloads such as HumanEval, MBPP, GSM8K, and MATH, while NLP classification and QA workloads show consis-

tent gains of 7.0–22.4%. Importantly, across all benchmarks, accuracy deviations remain within 1%, and LYNX often improves accuracy by upto 4%. For example, Qwen2-57B improves accuracy on MBPP (+0.8%) and TruthfulQA (+4.0%) while reducing latency by 16.8% and 17.3%, respectively. Mixtral-8×7B exhibits similar trends, with HumanEval accuracy increasing by 1.2% in addition to a 16.8% speedup, and CNN/DailyMail showing a 22.4% latency reduction with a 0.3% accuracy gain. DeepSeek-V2-Lite also benefits consistently, achieving 10–11% throughput gains across MATH and GSM8K with up to +1.2% accuracy on HumanEval.²

Two broader trends emerge. First, accuracy is stable under LYNX and often improves across benchmarks, suggesting that batching often invokes experts amenable for reduction in the vanilla baseline. Second, absolute latency savings grow with model size: larger models (e.g., Qwen2-57B and Mixtral-8×7B) achieve reductions of up to 6 ms/token, compared to ~1–2 ms/token for DeepSeek-V2-Lite. Taken together, these results demonstrate that LYNX delivers consistent gains while being iso-accurate, with the largest models experiencing the most improvements in throughput and often, accuracy.

5.3 Impact of Tuning

A key feature of LYNX is that it allows navigating the pareto frontier between accuracy and latency. Figure 11 (a) and (b) show how varying the two parameters, α and β , shape this trade-off. The findings are intuitive: throughput gains grow as α and β (§3.1) decrease, since the system is granted greater flexibility in treating experts as interchangeable. Importantly, accuracy constraints ultimately bound these gains, with conservative settings yielding 10–15% speedups under $\pm 1\%$ accuracy, while more aggressive configurations push savings to 20–25% by tolerating $\sim 5\%$ accuracy loss.

Between these regimes, α plays the stronger role by controlling how finely we distinguish near-top experts, while β provides complementary shaping by truncating the influence of lower-probability experts. Together, they offer smooth and interpretable control, enabling LYNX to operate either in a safe regime of modest gains or in an aggressive regime that unlocks larger speedups at controlled accuracy cost.

5.4 Enhancing Offloading Techniques

For memory constrained scenarios, MoE offloading techniques offload part of the model from the GPU memory onto the CPU memory. We evaluate two such techniques when running Mixtral on a single A100 GPU with 19GB out of 94GB offloaded to CPU memory. Since LYNX reduces the number of activated experts per batch, it is fully complimentary to techniques that offload model weights to the CPU memory. Conventional offloading techniques put fetch of the model weights from CPU DRAM to GPU in the critical path of the

²Benchmarks such as CNN/DailyMail and NarrativeQA are characterized by very high prefill to decode ratio, thereby exhibiting a lower baseline throughput as well.

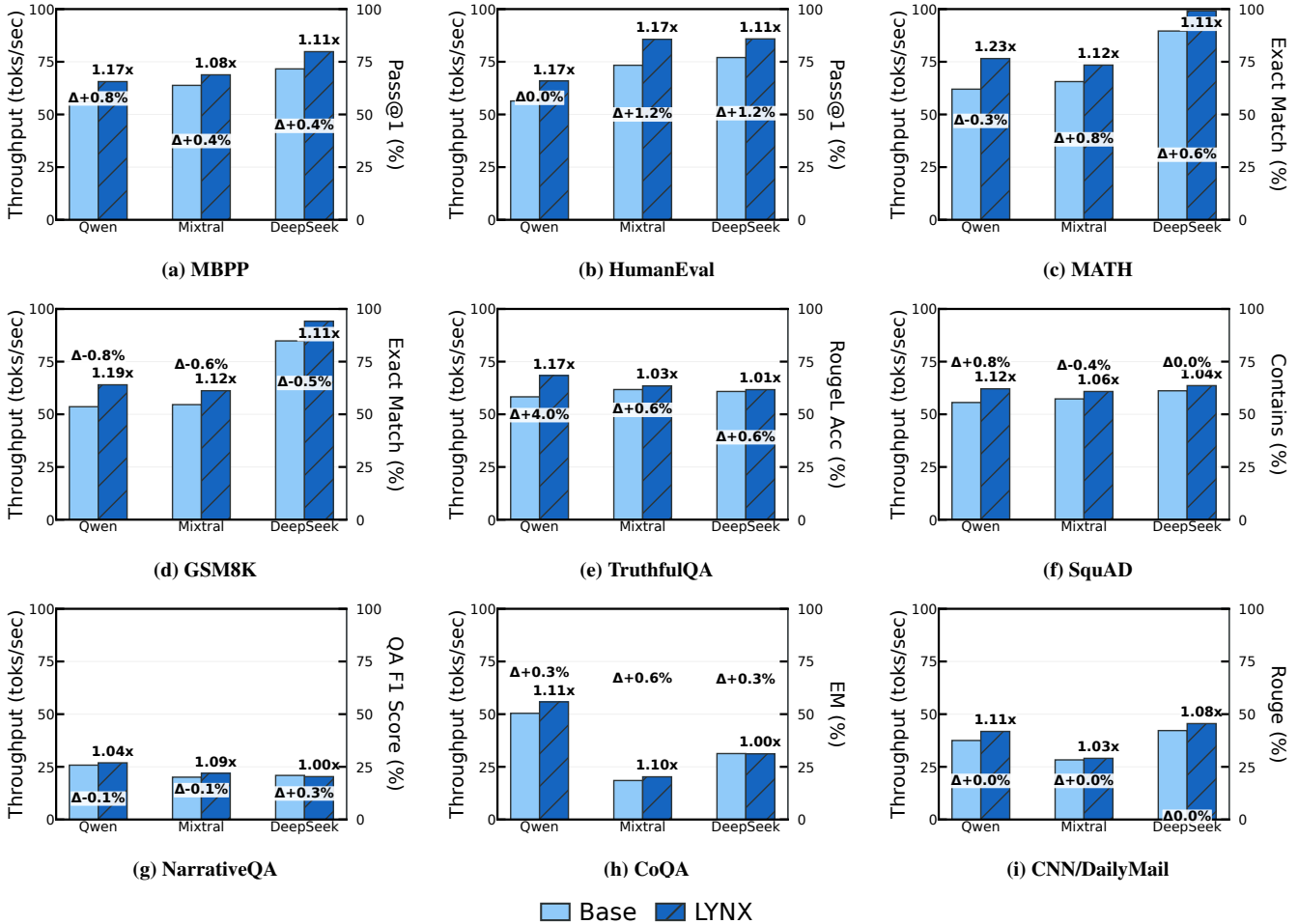


Figure 10: LYNX performance across diverse benchmarks. Bars show throughput (throughput in tokens/s) compared to SOTA vllm model serving and LYNX implementations across three models: Mixtral-8x7B-Instruct, DeepSeek-V2-Lite, and Qwen2-57B-A14B-Instruct. Speedup factors (e.g., 1.17 \times) are shown above LYNX bars. The secondary Y axis shows the corresponding accuracy metric and accuracy changes (Δ) are annotated, where positive values indicate accuracy improvements with LYNX.

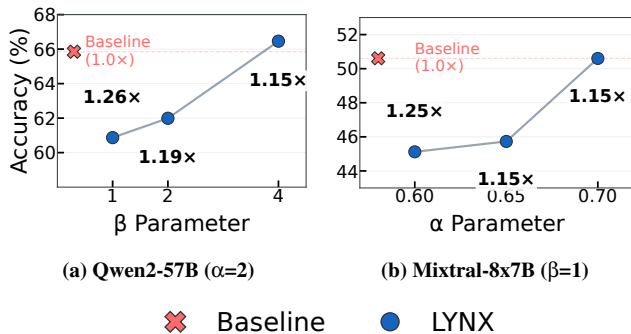


Figure 11: LYNX allows for graceful trade-off between accuracy and throughput speedup for HumanEval. More aggressive configuration parameters allow of navigating the Pareto-curve

decode latency. The transfer of model weights is bottlenecked by the limited PCIe bandwidth (32GB/s each direction in A100), making offloading about 50x slower than on-device

inference. LYNX reduces the activated experts per batch and hence the dominant data transfer of model weights. Even with 75% activated experts, which is the case for most benchmarks showcased above, LYNX improves the performance over vanilla offloading by 1.31 \times (Figure 12 left).

Fiddler [26], a recent offloading technique, exploits the availability of additional resources in the CPU to reduce offloading overheads, by computing the offloaded experts on the CPU and only transferring the activation tensors. As the activation tensors are 100x smaller in size compared to model weights (for small batch sizes), the critical path becomes the expert computation on the CPU, which is bottlenecked by the CPU bandwidth. For a typical 4-channel DDR5 system, the CPU bandwidth is about 160GB/s (40GB/s per channel), and computing 2 experts on the CPU requires about 10x longer than on an A100 GPU (with 1.5TB/s HBM bandwidth). Nonetheless, Fiddler improves over vanilla offloading by providing a 5x latency improvement. PROWL further enhances

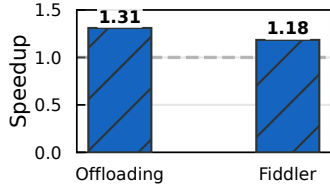


Figure 12: LYNX can enhance offloading techniques

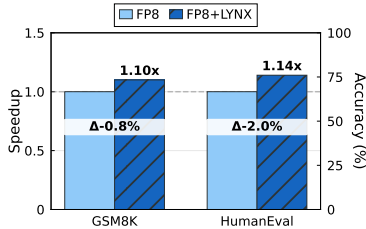


Figure 13: LYNX with Quantized models. Applying LYNX on top of fp8 quantized variants of Mixtral-Instruct-8x7B-v0.1 gives us a added throughput improvements of 10-14% points on top of the quantized model while maintaining similar accuracy

Fiddler by reducing the activated experts in CPU by 25%, resulting in a latency benefit of 1.38x compared to Fiddler alone. Overall, PROWL seamlessly improves the performance of both conventional and state-of-the-art offloading techniques.

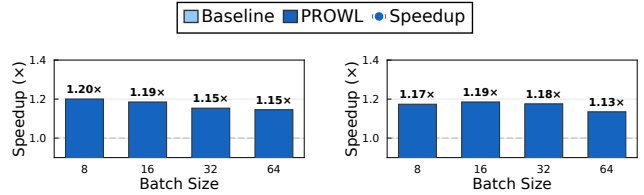
5.5 Enhancing Quantization Techniques

Recent quantization techniques accelerate MoE serving by pruning the model weights from FP32 and FP16 to FP8 or even lower [18], thereby reducing the data transfer overhead of model weights. LYNX is complimentary to quantization, as our technique reduces the number of activated experts, further reducing data transfer, even for quantized weights. For instance, LLM Compressor allows quantizing recent MoEs to FP8 using SmoothQuant and AWQ and is supported by our evaluation framework, vLLM.

We evaluate LYNX with Mixtral quantized to FP8 using SmoothQuant. As shown in Figure 13, LYNX provides 10-14% speedup at negligible drop in accuracy of 2.8% for GSM8K, and 1.2% for HumanEval. Other existing works employ online dynamic pruning on top of extreme quantization [18]. While such techniques provide significant latency benefit, on hard tasks such as GSM8k and HumanEval their accuracy drops vary drastically and therefore we didn't include them in our analysis. We believe that LYNX can be extended to any existing quantization schemes and show similar performance benefit.

5.6 Impact of Batch Size & Sequence Length

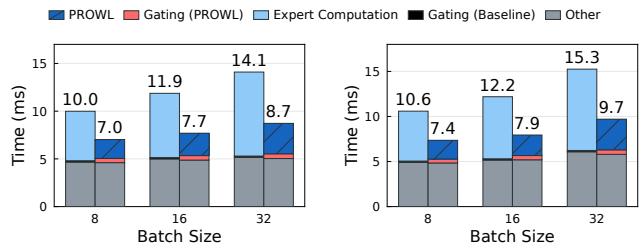
Figure 14 reports how LYNX's gains vary across batch sizes on GSM8K (left) and HumanEval (right). The findings are intuitive: TPOT improvements increase with batch size up to a point, after which they begin to saturate. On GSM8K, LYNX delivers its strongest benefits at moderate batch sizes, achieving over 1.20x speedup at batch size 8 and 1.19x at



(a) GSM8K

(b) HumanEval

Figure 14: Batch scalability for Qwen2 showing accuracy and speedup across different batch sizes. PROWL maintains comparable accuracy while achieving consistent 1.15-1.20x speedup.



(a) Sequence length 512

(b) Sequence length 4096

Figure 15: Latency breakdown for baseline and LYNX (for Qwen2) at different batch sizes. Red percentages indicate LYNX's overhead as a fraction of baseline's total time (3-4%). LYNX's overheads are low and don't grow with batch size.

batch size 16, before stabilizing near 1.15x at 32 and 64. HumanEval shows the same trend, with speedups climbing to 1.19x at batch size 16 and remaining in the 1.13–1.18x range thereafter. Importantly, these improvements hold consistently across benchmarks with different prefill to decode ratios. Overall, these results demonstrate that LYNX achieves robust latency reductions across tasks, with particularly strong benefits at moderate batch sizes before saturating, underscoring its effectiveness in practical deployment regimes.

5.7 Overheads & scalability

Figure 15 profiles the breakdown of end-to-end latency across expert and non-expert components. We observe that expert computation accounts for roughly 60% of total runtime. Thus, it is especially important that the routing mechanism itself does not erode potential gains. Considerable effort went into ensuring this: whereas a vanilla PyTorch implementation of our logic would require launching more than 700 kernels, our fused Triton kernels execute the entire routing procedure with only a 4% overheads. The remaining overheads, such as lightweight book-keeping at each layer, are negligible compared to expert execution. Taken together, these results show that LYNX's routing is extremely lightweight, allowing its latency savings from expert reduction to be fully realized in practice. Moreover, most LLM serving engines and libraries optimize the expert computation kernels for the total number of experts to select kernel dispatch parameters such as tile shape and group size. Further tuning of dispatch parameters for variable number of experts can lead to even higher gains.

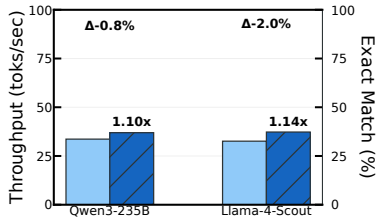


Figure 16: Dropping in LYNX on off-the-shelf recent releases (Llama 4 and Qwen 3 in this case, which are highly tuned for optimized expert selection) accelerates them on GSM8k.

5.8 LYNX on Recently Released Models

The popularity of MoEs have led to frequent new releases of highly optimized models. To showcase LYNX’s plug-and-play nature, we run it on two off-the-shelf SoTA models, Qwen3 and LLAMA4, without any characterization or tuning. As Figure 16 shows, LYNX provides 10-14% speedup with less than 2% accuracy degradation on the challenging GSM8K task. We note that tuning α and β will allow us to trade off accuracy for even more performance. Thus, we believe that LYNX can benefit any current or future MoEs.

6 Related Work

Static Expert Pruning and Fine-tuning. Early approaches create reduced MoE variants through static pruning [34]. Expert merging based on similarity observed among the outputs generated by experts is used to group ‘similar’ experts which are then merged using recent model merging techniques. While this opens a new dimension of expert reduction, finding all such combinations can be exceedingly time and resource consuming for MoEs with large number of experts. SEER-MoE [41] extends this through sparsification and regularized fine-tuning, while others employ evolutionary search [12, 17, 60] for expert reduction. However, these methods require task-specific calibration or fine-tuning overhead.

Dynamic Expert Management. Some techniques also enable dynamic expert reduction but these are limited to reducing the number of experts activated per token [18, 38]. While this can reduce the latency for single batch size, these latency improvements do not scale with increase in batch size. Recent work explores dynamic runtime expert activation based on relative importance of each token which is used as a threshold to decide how many experts will be selected per token. However, these approaches struggle with batch serving where activation patterns inevitably result in full expert utilization.

Model Compression. Compression techniques adapt pruning and quantization for MoEs [8, 18, 21, 60]. FP16/FP8 quantization [35, 52] can reduce memory footprint by 50-75%, at the expense of accuracy trade-offs. For example, for many large models which cannot fit in the GPU HBM, relying on quantized models with FP8 and even more extreme width quantization like 2-bit and 3-bit width. Such techniques can bring down the model size and improve model latency. We

show that LYNX complements quantization and such compression approaches for latency-sensitive deployments.

Expert Placement and Execution. Several systems focus on efficient expert distribution across devices. GShard [32] introduces expert parallelism. Recent work [20] optimizes communication through dynamic gating. Systems like [7] explore predictive expert pre-fetching, enabling CPU-GPU expert management [13, 53]. LYNX’s approach is complementary to Fiddler [26] and MoESys [16] which optimize expert placement for resource-constrained environments.

Speculative Decoding. A key technique to accelerate low latency LLM serving is by speculating multiple tokens using a *draft* model which the large *target* LLM can verify in a single step, thereby outputting more than one output token per sequence at each iteration. We observe that speculative decoding would lead to more experts being activated than in a non-speculative baseline, diminishing its gains. LYNX is complimentary to speculative decoding, as it would reduce the activated experts during speculation, leading to lower overhead of verification during speculation. [37]

Model Offloading and CPU execution. Fiddler [26] explores placing less-activated experts to CPU memory, fetching experts on-demand to the GPU in memory-constrained settings to mitigate weight transfer overhead for latency gains. Cache-conditional experts [49] modifies the router function to be conditioned on the device placement of model weights to bias selection of experts already in device memory, yielding increased generation throughput. Moe-Infinity [54] looks at commodity hardware settings which exhibit high degrees of expert activation sparsity due to singleton batches and then exploits online activation traces to perform pre-fetching of model weights into an expert cache and improve latency.

Pipelining and Overlapping. Klotski [15] addresses the problem of pipeline bubbles in MoE inference due to differences in IO (fetching offloaded weights) and execution latencies per layer. By using expert activation patterns to perform multi-batching and reordering expert execution schedule to better overlap computation with communication, inference pipeline bubbles are reduced, increasing throughput.

Additionally, we provide a summary of comparisons in §B.

7 Conclusion

We present LYNX, the first workload agnostic system to our best knowledge that accelerates MoE inference by relieving the fundamental tension in MoE between batching and selective parameter activation. The key to LYNX’s ability is its lightweight run-time batch-level dynamic expert remapping, informed by the key observations on MoEs that we revealed in this work, that reduces the number of experts required for that batch. LYNX boosts the performance of the state-of-the-art models from popular families by up to 1.23 \times on nine benchmarks without compromising on accuracy. Further, LYNX’s

complementary nature makes it easy to apply atop existing techniques to further improve their performance.

References

- [1] OpenAI Josh Achiam, Steven Adler, Sandhini Agarwal, Lama Ahmad, Ilge Akkaya, Florencia Leoni Aleman, Diogo Almeida, Janko Altenschmidt, Sam Altman, Shyamal Anadkat, Red Avila, Igor Babuschkin, Suchir Balaji, Valerie Balcom, Paul Baltescu, Haiming Bao, Mo Bavarian, Jeff Belgum, Irwan Bello, Jake Berdine, Gabriel Bernadett-Shapiro, Christopher Berner, Lenny Bogdonoff, Oleg Boiko, Madeleine Boyd, Anna-Luisa Brakman, Greg Brockman, Tim Brooks, Miles Brundage, Kevin Button, Trevor Cai, Rosie Campbell, Andrew Cann, Brittany Carey, Chelsea Carlson, Rory Carmichael, Brooke Chan, Che Chang, Fotis Chantzis, Derek Chen, Sully Chen, Ruby Chen, Jason Chen, Mark Chen, Benjamin Chess, Chester Cho, Casey Chu, Hyung Won Chung, Dave Cummings, Jeremiah Currier, Yunxing Dai, Cory Decareaux, Thomas Degry, Noah Deutsch, Damien Deville, Arka Dhar, David Dohan, Steve Dowling, Sheila Dunning, Adrien Ecoffet, Atty Eleti, Tyna Eloundou, David Farhi, Liam Fedus, Niko Felix, Simón Posada Fishman, Juston Forte, Isabella Fulford, Leo Gao, Elie Georges, Christian Gibson, Vik Goel, Tarun Gogineni, Gabriel Goh, Raphael Gontijo-Lopes, Jonathan Gordon, Morgan Grafstein, Scott Gray, Ryan Greene, Joshua Gross, Shixiang Shane Gu, Yufei Guo, Chris Hallacy, Jesse Han, Jeff Harris, Yuchen He, Mike Heaton, Johannes Heidecke, Chris Hesse, Alan Hickey, Wade Hickey, Peter Hoeschele, Brandon Houghton, Kenny Hsu, Shengli Hu, Xin Hu, Joost Huizinga, Shantanu Jain, Shawn Jain, Joanne Jang, Angela Jiang, Roger Jiang, Haozhun Jin, Denny Jin, Shino Jomoto, Billie Jonn, Heewoo Jun, Tomer Kaftan, Lukasz Kaiser, Ali Kamali, Ingmar Kanitscheider, Nitish Shirish Keskar, Tabarak Khan, Logan Kilpatrick, Jong Wook Kim, Christina Kim, Yongjik Kim, Hendrik Kirchner, Jamie Ryan Kiros, Matthew Knight, Daniel Kokotajlo, Lukasz Kondraciuk, Andrew Kondrich, Aris Konstantinidis, Kyle Kosic, Gretchen Krueger, Vishal Kuo, Michael Lampe, Ikai Lan, Teddy Lee, Jan Leike, Jade Leung, Daniel Levy, Chak Li, Rachel Lim, Molly Lin, Stephanie Lin, Mateusz Litwin, Theresa Lopez, Ryan Lowe, Patricia Lue, Anna Makanju, Kim Malfacini, Sam Manning, Todor Markov, Yaniv Markovski, Bianca Martin, Katie Mayer, Andrew Mayne, Bob McGrew, Scott Mayer McKinney, Christine McLeavey, Paul McMillan, Jake McNeil, David Medina, Aalok Mehta, Jacob Menick, Luke Metz, Andrey Mishchenko, Pamela Mishkin, Vinnie Monaco, Evan Morikawa, Daniel P. Mossing, Tong Mu, Mira Murati, Oleg Murk, David N. M. S. e. ly, Ashvin Nair, Reiichiro Nakano, Rajeev Nayak, Arvind Neelakantan, Richard Ngo, Hyeonwoo Noh, Ouyang Long, Cullen O’Keefe, Jakub W. Pachocki, Alex Paino, Joe Palermo, Ashley Pantuliano, Giambattista Parascandolo, Joel Parish, Emy Parparita, Alexandre Passos, Mikhail Pavlov, Andrew Peng, Adam Perelman, Filipe de Avila Belbute Peres, Michael Petrov, Henrique Pondé de Oliveira Pinto, Michael Pookorny, Michelle Pokrass, Vitchyr H. Pong, Tolly Powell, Alethea Power, Boris Power, Elizabeth Proehl, Raul Puri, Alec Radford, Jack W. Rae, Aditya Ramesh, Cameron Raymond, Francis Real, Kendra Rimbach, Carl Ross, Bob Rotsted, Henri Roussez, Nick Ryder, Mario D. Saltarelli, Ted Sanders, Shibani Santurkar, Girish Sastry, Heather Schmidt, David Schnurr, John Schulman, Daniel Selsam, Kyla Sheppard, Toki Sherbakov, Jessica Shieh, Sarah Shoker, Pranav Shyam, Szymon Sidor, Eric Sigler, Maddie Simens, Jordan Sitkin, Katarina Slama, Ian Sohl, Benjamin Sokolowsky, Yang Song, Natalie Staudacher, Felipe Petroski Such, Natalie Summers, Ilya Sutskever, Jie Tang, Nikolas A. Tezak, Madeleine Thompson, Phil Tillet, Amin Tootoonchian, Elizabeth Tseng, Preston Tuggle, Nick Turley, Jerry Tworek, Juan Felipe Cerón Uribe, Andrea Vallone, Arun Vijayvergiya, Chelsea Voss, Carroll L. Wainwright, Justin Jay Wang, Alvin Wang, Ben Wang, Jonathan Ward, Jason Wei, CJ Weinmann, Akila Welihinda, Peter Welinder, Jiayi Weng, Lilian Weng, Matt Wiethoff, Dave Willner, Clemens Winter, Samuel Wolrich, Hannah Wong, Lauren Workman, Sherwin Wu, Jeff Wu, Michael Wu, Kai Xiao, Tao Xu, Sarah Yoo, Kevin Yu, Qiming Yuan, Wojciech Zaremba, Rowan Zellers, Chong Zhang, Marvin Zhang, Shengjia Zhao, Tianhao Zheng, Juntang Zhuang, William Zhuk, and Barret Zoph. Gpt-4 technical report. 2023.
- [2] Amey Agrawal, Nitin Kedia, Jayashree Mohan, Ashish Panwar, Nipun Kwatra, Bhargav S. Gulavani, Ramachandran Ramjee, and Alexey Tumanov. Vidur: A large-scale simulation framework for llm inference. *ArXiv*, abs/2405.05465, 2024.
- [3] Amey Agrawal, Nitin Kedia, Ashish Panwar, Jayashree Mohan, Nipun Kwatra, Bhargav S. Gulavani, Alexey Tumanov, and Ramachandran Ramjee. Taming throughput-latency tradeoff in llm inference with sarathi-serve. *ArXiv*, abs/2403.02310, 2024.
- [4] Anthropic. Claude, 2024. Accessed: 2024-10-31.
- [5] Jacob Austin, Augustus Odena, Maxwell Nye, Maarten Bosma, Henryk Michalewski, David Dohan, Ellen Jiang, Carrie Cai, Michael Terry, Quoc Le, and Charles Sutton. Program synthesis with large language models, 2021.
- [6] Mark Chen, Jerry Tworek, Heewoo Jun, Qiming Yuan, Henrique Pondé, Jared Kaplan, Harrison Edwards, Yura Burda, Nicholas Joseph, Greg Brockman, Alex Ray,

- Raul Puri, Gretchen Krueger, Michael Petrov, Heidy Khlaaf, Girish Sastry, Pamela Mishkin, Brooke Chan, Scott Gray, Nick Ryder, Mikhail Pavlov, Alethea Power, Lukasz Kaiser, Mohammad Bavarian, Clemens Winter, Philippe Tillet, Felipe Petroski Such, David W. Cummings, Matthias Plappert, Fotios Chantzis, Elizabeth Barnes, Ariel Herbert-Voss, William H. Guss, Alex Nichol, Igor Babuschkin, Suchir Balaji, Shantanu Jain, Andrew Carr, Jan Leike, Joshua Achiam, Vedant Misra, Evan Morikawa, Alec Radford, Matthew M. Knight, Miles Brundage, Mira Murati, Katie Mayer, Peter Welinder, Bob McGrew, Dario Amodei, Sam McCandlish, Ilya Sutskever, and Wojciech Zaremba. Evaluating large language models trained on code. *ArXiv*, abs/2107.03374, 2021.
- [7] Tianyu Chen, Shaohan Huang, Yuan Xie, Binxing Jiao, Daxin Jiang, Haoyi Zhou, Jianxin Li, and Furu Wei. Task-specific expert pruning for sparse mixture-of-experts. *ArXiv*, abs/2206.00277, 2022.
- [8] Yuanteng Chen, Yuantian Shao, Peisong Wang, and Jian Cheng. Eac-moe: Expert-selection aware compressor for mixture-of-experts large language models. *ArXiv*, abs/2508.01625, 2025.
- [9] Aidan Clark, Diego de Las Casas, Aurelia Guy, Arthur Mensch, Michela Paganini, Jordan Hoffmann, Bogdan Damoc, Blake A. Hechtman, Trevor Cai, Sebastian Borgeaud, George van den Driessche, Eliza Rutherford, T. W. Hennigan, Matthew G. Johnson, Katie Millican, Albin Cassirer, Chris Jones, Elena Buchatskaya, David Budden, L. Sifre, Simon Osindero, Oriol Vinyals, Jack W. Rae, Erich Elsen, Koray Kavukcuoglu, and Karen Simonyan. Unified scaling laws for routed language models. In *International Conference on Machine Learning*, 2022.
- [10] Karl Cobbe, Vineet Kosaraju, Mohammad Bavarian, Mark Chen, Heewoo Jun, Lukasz Kaiser, Matthias Plappert, Jerry Tworek, Jacob Hilton, Reiichiro Nakano, Christopher Hesse, and John Schulman. Training verifiers to solve math word problems. *ArXiv*, abs/2110.14168, 2021.
- [11] DeepSeek-AI, Aixin Liu, Bei Feng, Bing Xue, Bing-Li Wang, Bochao Wu, Chengda Lu, Chenggang Zhao, Chengqi Deng, Chenyu Zhang, Chong Ruan, Damai Dai, Daya Guo, Dejian Yang, Deli Chen, Dong-Li Ji, Erhang Li, Fangyun Lin, Fucong Dai, Fuli Luo, Guangbo Hao, Guanting Chen, Guowei Li, H. Zhang, Han Bao, Hanwei Xu, Haocheng Wang, Haowei Zhang, Honghui Ding, Huajian Xin, Huazuo Gao, Hui Li, Hui Qu, J. L. Cai, Jian Liang, Jianzhong Guo, Jiaqi Ni, Jiashi Li, Jiawei Wang, Jin Chen, Jingchang Chen, Jingyang Yuan, Junjie Qiu, Junlong Li, Jun-Mei Song, Kai Dong, Kai Hu, Kaige Gao, Kang Guan, Kexin Huang, Kuai Yu, Lean Wang, Lecong Zhang, Lei Xu, Leyi Xia, Liang Zhao, Litong Wang, Liyue Zhang, Meng Li, Miaojun Wang, Mingchuan Zhang, Minghua Zhang, Minghui Tang, Mingming Li, Ning Tian, Panpan Huang, Peiyi Wang, Peng Zhang, Qiancheng Wang, Qihao Zhu, Qinyu Chen, Qiushi Du, R. J. Chen, R. L. Jin, Ruiqi Ge, Ruisong Zhang, Ruizhe Pan, Runji Wang, Runxin Xu, Ruoyu Zhang, Ruyi Chen, S. S. Li, Shanghao Lu, Shangyan Zhou, Shanhuang Chen, Shao-Ping Wu, Shengfeng Ye, Shirong Ma, Shiyu Wang, Shuang Zhou, Shuiping Yu, Shunfeng Zhou, Shuting Pan, T. Wang, Tao Yun, Tian Pei, Tianyu Sun, W. L. Xiao, Wangding Zeng, Wan-jia Zhao, Wei An, Wen Liu, Wenfeng Liang, Wenjun Gao, Wen-Xuan Yu, Wentao Zhang, X. Q. Li, Xiangyu Jin, Xianzu Wang, Xiaoling Bi, Xiaodong Liu, Xiaohan Wang, Xi-Cheng Shen, Xiaokang Chen, Xiaokang Zhang, Xiaosha Chen, Xiaotao Nie, Xiaowen Sun, Xiaoxiang Wang, Xin Cheng, Xin Liu, Xin Xie, Xingchao Liu, Xingkai Yu, Xinnan Song, Xinxia Shan, Xinyi Zhou, Xinyu Yang, Xinyuan Li, Xuecheng Su, Xuheng Lin, Y. K. Li, Y. Q. Wang, Y. X. Wei, Y. X. Zhu, Yang Zhang, Yanhong Xu, Yanping Huang, Yao Li, Yao Zhao, Yaofeng Sun, Yao Li, Yaohui Wang, Yi Yu, Yi Zheng, Yichao Zhang, Yifan Shi, Yi Xiong, Ying He, Ying Tang, Yishi Piao, Yisong Wang, Yixuan Tan, Yi-Bing Ma, Yiyuan Liu, Yongqiang Guo, Yu Wu, Yuan Ou, Yuchen Zhu, Yudian Wang, Yue Gong, Yuheng Zou, Yujia He, Yukun Zha, Yunfan Xiong, Yunxiang Ma, Yuting Yan, Yu-Wei Luo, Yu mei You, Yuxuan Liu, Yuyang Zhou, Z. F. Wu, Zehui Ren, Zehui Ren, Zhangli Sha, Zhe Fu, Zhean Xu, Zhen Huang, Zhen Zhang, Zhenda Xie, Zhen guo Zhang, Zhewen Hao, Zhibin Gou, Zhicheng Ma, Zhigang Yan, Zhihong Shao, Zhipeng Xu, Zhiyu Wu, Zhongyu Zhang, Zhuoshu Li, Zihui Gu, Zijia Zhu, Zijun Liu, Zi-An Li, Ziwei Xie, Ziyang Song, Ziyi Gao, and Zizheng Pan. Deepseek-v3 technical report. *ArXiv*, abs/2412.19437, 2024.
- [12] Zican Dong, Han Peng, Peiyu Liu, Wayne Xin Zhao, Dong Wu, Feng Xiao, and Zhifeng Wang. Domain specific pruning of large mixture-of-experts models with few-shot demonstrations, 2025.
- [13] Artyom Eliseev and Denis Mazur. Fast inference of mixture-of-experts language models with offloading. *ArXiv*, abs/2312.17238, 2023.
- [14] Amr Elmeleegy, Harry Kim, David Zier, Kyle Kranen, Neelay Shah, Ryan Olson, and Omri Kahalon. Nvidia dynamo: A low-latency distributed inference framework for scaling reasoning ai models. Blog post, NVIDIA Developer, March 2025. Available at: <https://developer.nvidia.com/blog/introducing-nvidia-dynamo-a-low-latency-distributed-inference-framework-for-scaling-reasoning-ai-models>.

- [15] Zhiyuan Fang, Yuegui Huang, Zicong Hong, Yufeng Lyu, Wuhui Chen, Yue Yu, Fan Yu, and Zibin Zheng. Klotski: Efficient mixture-of-expert inference via expert-aware multi-batch pipeline, 2025.
- [16] William Fedus, Barret Zoph, and Noam Shazeer. Switch transformers: scaling to trillion parameter models with simple and efficient sparsity. *J. Mach. Learn. Res.*, 23(1), jan 2022.
- [17] En hao Liu, Junyi Zhu, Zinan Lin, Xuefei Ning, Matthew B. Blaschko, Shengen Yan, Guohao Dai, Huazhong Yang, and Yu Wang. Efficient expert pruning for sparse mixture-of-experts language models: Enhancing performance and reducing inference costs. 2024.
- [18] Shwai He, Daize Dong, Liang Ding, and Ang Li. Demystifying the compression of mixture-of-experts through a unified framework, 2024.
- [19] Karl Moritz Hermann, Tomáš Kočiský, Edward Grefenstette, Lasse Espeholt, Will Kay, Mustafa Suleyman, and Phil Blunsom. Teaching machines to read and comprehend. In *Advances in Neural Information Processing Systems*, volume 28, 2015.
- [20] Haiyang Huang, Newsha Ardalani, Anna Sun, Liu Ke, Hsien-Hsin S. Lee, Anjali Sridhar, Shruti Bhosale, Carole-Jean Wu, and Benjamin Lee. Towards moe deployment: Mitigating inefficiencies in mixture-of-expert (moe) inference. *ArXiv*, abs/2303.06182, 2023.
- [21] Wei Huang, Yue Liao, Jianhui Liu, Ruifei He, Haoru Tan, Shiming Zhang, Hongsheng Li, Si Liu, and XIAOJUAN QI. Mixture compressor for mixture-of-experts LLMs gains more. In *The Thirteenth International Conference on Learning Representations*, 2025.
- [22] Changho Hwang, Wei Cui, Yifan Xiong, Ziyue Yang, Ze Liu, Han Hu, Zilong Wang, Rafael Salas, Jithin Jose, Prabhat Ram, Joe Chau, Peng Cheng, Fan Yang, Mao Yang, and Yongqiang Xiong. Tutel: Adaptive mixture-of-experts at scale. *ArXiv*, abs/2206.03382, 2022.
- [23] Ranggi Hwang, Jianyu Wei, Shijie Cao, Changho Hwang, Xiaohu Tang, Ting Cao, Mao Yang, and Minsoo Rhu. Pre-gated moe: An algorithm-system co-design for fast and scalable mixture-of-expert inference. *2024 ACM/IEEE 51st Annual International Symposium on Computer Architecture (ISCA)*, pages 1018–1031, 2023.
- [24] Ajay Jaiswal, Jianyu Wang, Yixiao Li, Pingzhi Li, Tianlong Chen, Zhangyang Wang, Chong Wang, Ruoming Pang, and Xianzhi Du. Finding fantastic experts in moes: A unified study for expert dropping strategies and observations. *arXiv preprint arXiv:2504.05586*, 2025.
- [25] Albert Q. Jiang, Alexandre Sablayrolles, Antoine Roux, Arthur Mensch, Blanche Savary, Chris Bamford, Devendra Singh Chaplot, Diego de Las Casas, Emma Bou Hanna, Florian Bressand, Gianna Lengyel, Guillaume Bour, Guillaume Lample, L’elio Renard Lavaud, Lucile Saulnier, Marie-Anne Lachaux, Pierre Stock, Sandeep Subramanian, Sophia Yang, Szymon Antoniak, Teven Le Scao, Théophile Gervet, Thibaut Lavril, Thomas Wang, Timothée Lacroix, and William El Sayed. Mixtral of experts. *ArXiv*, abs/2401.04088, 2024.
- [26] Keisuke Kamahori, Yile Gu, Kan Zhu, and Baris Kasikci. Fiddler: Cpu-gpu orchestration for fast inference of mixture-of-experts models. *ArXiv*, abs/2402.07033, 2024.
- [27] Tomáš Kočiský, Jonathan Schwarz, Phil Blunsom, Chris Dyer, Karl Moritz Hermann, Gábor Melis, and Edward Grefenstette. The NarrativeQA reading comprehension challenge. *Transactions of the Association for Computational Linguistics*, 6:317–328, 2018.
- [28] Jakub Krajewski, Jan Ludziejewski, Kamil Adamczewski, Maciej Pi’oro, Michal Krutul, Szymon Antoniak, Kamil Ciebiera, Krystian Kr’ol, Tomasz Odrzyg’o’zd’z, Piotr Sankowski, Marek Cygan, and Sebastian Jaszczur. Scaling laws for fine-grained mixture of experts. *ArXiv*, abs/2402.07871, 2024.
- [29] Kyle Kranen and Vinh Nguyen. Applying mixture of experts in llm architectures. <https://developer.nvidia.com/blog/applying-mixture-of-experts-in-llm-architectures/>, March 2024. NVIDIA Developer Blog.
- [30] Woosuk Kwon, Zhuohan Li, Siyuan Zhuang, Ying Sheng, Lianmin Zheng, Cody Hao Yu, Joseph E. Gonzalez, Hao Zhang, and Ion Stoica. Efficient memory management for large language model serving with page-dattention. In *Proceedings of the ACM SIGOPS 29th Symposium on Operating Systems Principles*, 2023.
- [31] Jaeseong Lee, Aurick Qiao, Daniel F Campos, Zhewei Yao, Yuxiong He, et al. Stun: Structured-then-unstructured pruning for scalable moe pruning. *arXiv preprint arXiv:2409.06211*, 2024.
- [32] Dmitry Lepikhin, HyoukJoong Lee, Yuanzhong Xu, Dehao Chen, Orhan Firat, Yanping Huang, Maxim Krikun, Noam M. Shazeer, and Z. Chen. Gshard: Scaling giant models with conditional computation and automatic sharding. *ArXiv*, abs/2006.16668, 2020.
- [33] Aitor Lewkowycz, Anders Andreassen, David Dohan, Ethan Dyer, Henryk Michalewski, Vinay Ramasesh, Ambrose Slone, Cem Anil, Imanol Schlag, Theo Gutman-Solo, Yuhuai Wu, Behnam Neyshabur, Guy Gur-Ari, and Vedant Misra. Solving quantitative reasoning problems with language models, 2022.

- [34] Pingzhi Li, Zhenyu (Allen) Zhang, Prateek Yadav, Yi-Lin Sung, Yu Cheng, Mohit Bansal, and Tianlong Chen. Merge, then compress: Demystify efficient smoe with hints from its routing policy. *ArXiv*, abs/2310.01334, 2023.
- [35] Ji Lin, Jiaming Tang, Haotian Tang, Shang Yang, Weiming Chen, Wei-Chen Wang, Guangxuan Xiao, Xingyu Dang, Chuang Gan, and Song Han. Awq: Activation-aware weight quantization for llm compression and acceleration. In *MLSys*, 2024.
- [36] Stephanie Lin, Jacob Hilton, and Owain Evans. TruthfulQA: Measuring how models mimic human falsehoods. In Smaranda Muresan, Preslav Nakov, and Aline Villavicencio, editors, *Proceedings of the 60th Annual Meeting of the Association for Computational Linguistics (Volume 1: Long Papers)*, pages 3214–3252, Dublin, Ireland, May 2022. Association for Computational Linguistics.
- [37] Xiaoxuan Liu, Cade Daniel, Langxiang Hu, Woosuk Kwon, Zhuohan Li, Xiangxi Mo, Alvin Cheung, Zhijie Deng, Ion Stoica, and Hao Zhang. Optimizing speculative decoding for serving large language models using goodput, 2024.
- [38] Xudong Lu, Qi Liu, Yuhui Xu, Aojun Zhou, Siyuan Huang, Bo Zhang, Junchi Yan, and Hongsheng Li. Not all experts are equal: Efficient expert pruning and skipping for mixture-of-experts large language models. *ArXiv*, abs/2402.14800, 2024.
- [39] Meta AI. Llama 4 models. <https://www.llama.com/models/llama-4/>, 2024. Accessed: 2025-04-17.
- [40] Mosaic. Introducing dbrx: A new state-of-the-art open llm, March 2024. Accessed: 2024-10-30.
- [41] Alexandre Muzio, Alex Sun, and Churan He. Seer-moe: Sparse expert efficiency through regularization for mixture-of-experts. *ArXiv*, abs/2404.05089, 2024.
- [42] NVIDIA. Fastertransformer. <https://github.com/NVIDIA/FasterTransformer>, 2023. GitHub repository.
- [43] OpenAI. Chatgpt. <https://chat.openai.com/>, 2022. Production-grade conversational AI service.
- [44] Pranav Rajpurkar, Jian Zhang, Konstantin Lopyrev, and Percy Liang. SQuAD: 100,000+ questions for machine comprehension of text. In Jian Su, Kevin Duh, and Xavier Carreras, editors, *Proceedings of the 2016 Conference on Empirical Methods in Natural Language Processing*, pages 2383–2392, Austin, Texas, November 2016. Association for Computational Linguistics.
- [45] Siva Reddy, Danqi Chen, and Christopher D. Manning. CoQA: A conversational question answering challenge. *Transactions of the Association for Computational Linguistics*, 7:249–266, 2019.
- [46] Zhihong Shao, Damai Dai, Daya Guo, Bo Liu (Benjamin Liu), Zihan Wang, and Huajian Xin. Deepseek-v2: A strong, economical, and efficient mixture-of-experts language model. *ArXiv*, abs/2405.04434, 2024.
- [47] Zhihong Shao, Damai Dai, Daya Guo, Bo Liu (Benjamin Liu), Zihan Wang, and Huajian Xin. Deepseek-v2: A strong, economical, and efficient mixture-of-experts language model. *ArXiv*, abs/2405.04434, 2024.
- [48] Noam M. Shazeer, Azalia Mirhoseini, Krzysztof Maziarz, Andy Davis, Quoc V. Le, Geoffrey E. Hinton, and Jeff Dean. Outrageously large neural networks: The sparsely-gated mixture-of-experts layer. *ArXiv*, abs/1701.06538, 2017.
- [49] Andrii Skliar, Ties van Rozendaal, Romain Lepert, Todor Boinovski, Mart van Baalen, Markus Nagel, Paul Whatmough, and Babak Ehteshami Bejnordi. Mixture of cache-conditional experts for efficient mobile device inference, 2024.
- [50] Jovan Stojkovic, Chaojie Zhang, Íñigo Goiri, Josep Torrellas, and Esha Choukse. Dynamollm: Designing llm inference clusters for performance and energy efficiency. *2025 IEEE International Symposium on High Performance Computer Architecture (HPCA)*, pages 1348–1362, 2024.
- [51] Philippe Tillet, Hsiang-Tsung Kung, and David Cox. Triton: an intermediate language and compiler for tiled neural network computations. In *Proceedings of the 3rd ACM SIGPLAN International Workshop on Machine Learning and Programming Languages*, pages 10–19, 2019.
- [52] Guangxuan Xiao, Ji Lin, Mickael Seznec, Hao Wu, Julien Demouth, and Song Han. SmoothQuant: Accurate and efficient post-training quantization for large language models. In *Proceedings of the 40th International Conference on Machine Learning*, 2023.
- [53] Leyang Xue, Yao Fu, Zhan Lu, Luo Mai, and Mahesh Marina. Moe-infinity: Activation-aware expert offloading for efficient moe serving. *ArXiv*, abs/2401.14361, 2024.
- [54] Leyang Xue, Yao Fu, Zhan Lu, Luo Mai, and Mahesh Marina. Moe-infinity: Efficient moe inference on personal machines with sparsity-aware expert cache, 2025.

- [55] An Yang, Baosong Yang, Binyuan Hui, Bo Zheng, Bowen Yu, Chang Zhou, Chengpeng Li, Chengyuan Li, Dayiheng Liu, Fei Huang, Guanting Dong, Haoran Wei, Huan Lin, Jialong Tang, Jialin Wang, Jian Yang, Jianhong Tu, Jianwei Zhang, Jianxin Ma, Jin Xu, Jingren Zhou, Jinze Bai, Jinzheng He, Junyang Lin, Kai Dang, Keming Lu, Ke-Yang Chen, Kexin Yang, Mei Li, Min Xue, Na Ni, Pei Zhang, Peng Wang, Ru Peng, Rui Men, Ruize Gao, Runji Lin, Shijie Wang, Shuai Bai, Sinan Tan, Tianhang Zhu, Tianhao Li, Tianyu Liu, Wenbin Ge, Xiaodong Deng, Xiaohuan Zhou, Xingzhang Ren, Xinyu Zhang, Xipin Wei, Xuancheng Ren, Yang Fan, Yang Yao, Yichang Zhang, Yunyang Wan, Yunfei Chu, Zeyu Cui, Zhenru Zhang, and Zhi-Wei Fan. Qwen2 technical report. *ArXiv*, abs/2407.10671, 2024.
- [56] Cheng Yang, Yang Sui, Jinqi Xiao, Lingyi Huang, Yu Gong, Yuanlin Duan, Wenqi Jia, Miao Yin, Yu Cheng, and Bo Yuan. Moe-i²: Compressing mixture of experts models through inter-expert pruning and intra-expert low-rank decomposition. In *Conference on Empirical Methods in Natural Language Processing*, 2024.
- [57] Gyeong-In Yu and Joo Seong Jeong. Orca: A distributed serving system for transformer-based generative models. In *USENIX Symposium on Operating Systems Design and Implementation*, 2022.
- [58] Hanfei Yu, Xingqi Cui, Hong Zhang, Hao Wang, and Hao Wang. fmoe: Fine-grained expert offloading for large mixture-of-experts serving. *ArXiv*, abs/2502.05370, 2025.
- [59] Longfei Yun, Yonghao Zhuang, Yao Fu, Eric P. Xing, and Hao Zhang. Toward inference-optimal mixture-of-expert large language models. *ArXiv*, abs/2404.02852, 2024.
- [60] Geng Zhang, Yuxuan Han, Yuxuan Lou, Wangbo Zhao, Yiqi Zhang, and Yang You. Mone: Replacing redundant experts with lightweight novices for structured pruning of moe. *ArXiv*, abs/2507.00390, 2025.
- [61] Yinmin Zhong, Shengyu Liu, Junda Chen, Jianbo Hu, Yibo Zhu, Xuanzhe Liu, Xin Jin, and Hao Zhang. Distserve: disaggregating prefill and decoding for goodput-optimized large language model serving. In *Proceedings of the 18th USENIX Conference on Operating Systems Design and Implementation*, OSDI’24, USA, 2024. USENIX Association.

A Design Details: Expert Binning

In this section we describe the expert binning policy (§3.1.1) of LYNX in more detail.

For each token, we subtract each expert’s router logit with the token’s maximum logit, scale this gap by the hyperparameter α , and round up to the nearest integer. This discretizes the router logits into integer values less than or equal to zero, effectively binning the experts based on how close their probabilities are to the top-1 expert.

Specifically, when softmax is used to convert router logits into probability weights, this design bins the experts based on the ratio of their probability with respect to the top-1 expert probability. A bin represented by an integer $-q$ would hold experts with probabilities within the range $(p_{max}/e^{q+1/\alpha}, p_{max}/e^{q/\alpha}]$, where p_{max} is the top-1 expert probability. For example, with $\alpha = 2$, it can be interpreted as treating experts that have probability ratios less than \sqrt{e} to be of roughly the same importance.

β marks the bin index from which all lower-probability experts are grouped together in one bin. Instead of using bins $-\beta, -\beta - 1, -\beta - 2$, and so on for progressively smaller probabilities, every expert whose probability falls in $[0, p_{max}/e^{\beta/\alpha}]$ is assigned to the same single bin $-\beta$. This means that we are ignoring the probability differences of all experts that have probability less than or equal to $p_{max}/e^{\beta/\alpha}$. Thus the ratio β/α never needs to exceed 3 and often not even 2, since experts with probabilities below $p_{max}/e^3 \simeq p_{max}/20$ contribute negligibly.

Some recent models (e.g. Llama4) use a sigmoid gate instead of softmax. In those cases we apply the same binning method to the pre-sigmoid scores.

B Summary of Comparisons

This table further highlights the differences between prior works and LYNX showcasing how our solution is light-weight, workload-agnostic and performant on complex tasks.

Technique	Workload agnostic	Calib. free	Complex Tasks	Plug & play	Disagg. Friendly
NAEE	✗	✗	✗	✗	✓
EASY-EP	✗	✗	✓	✗	✓
ODP	✗	✗	✗	✓	✗
PESF	✓	✓	✗	✓	✗
EEP	✗	✗	✗	✗	✓
MoNE	✗	✗	✗	✓	✓
Prowl (Ours)	✓	✓	✓	✓	✓